

## CAN ROCKY EXOPLANETS WITH RINGS POSE AS SUB-NEPTUNES?

ANTHONY L. PIRO

The Observatories of the Carnegie Institution for Science, 813 Santa Barbara St., Pasadena, CA 91101, USA; piro@carnegiescience.edu  
*Submitted for publication in The Astronomical Journal*

### ABSTRACT

In our solar system, the presence of rings is exclusive to the gas giants, but is this the case for all planetary systems? In principle, it seems that rocky exoplanets could also have rings, which could be searched for by studying their subtle imprint on the ingress and egress of transits. Unfortunately, such effects are difficult to measure and require high precision photometric and/or spectroscopic observations. At the most basic level though, the presence of rings would result in an increased transit depth that could be mistaken as an anonymously large radius. Motivated by this, I consider how a population of exoplanets with rings would impact radius measurements, focusing on Earth-like exoplanets. It is found that this population introduces an enhancement of inferred radii in the range of  $\sim 2 - 3R_{\oplus}$ , not unlike the sub-Neptunes that have been identified in recent transit surveys. Whether rings can explain all or most sub-Neptunes seems difficult, since it would require a large fraction of rocky planets to have rings ( $\gtrsim 50\%$ ) and/or a factor of  $\sim 2 - 3$  increase in the number of planets with radii  $\lesssim 1.2R_{\oplus}$ . Even if rings cannot explain all sub-Neptunes, this work suggests that focusing on those planets currently classified as sub-Neptunes may be a good starting place for finding rocky planets with rings.

*Subject headings:* occultations — planets and satellites: detection — planets and satellites: rings

### 1. INTRODUCTION

Rings are common amongst the four outer gas-rich planets in our solar system, while they are completely absent for the rocky planets. Nevertheless, if we have learned anything from the last two decades of exoplanet research, it is that other planetary systems find a way of repeatedly defying our expectations based on what we know from closer to home. This thus begs the question whether the terrestrial extrasolar planets, which are now known to be basically ubiquitous in our Galaxy (Burke et al. 2015; Mulders et al. 2015), actually sometimes have rings.

In fact, there are reasons to think that some rocky planets will have rings. Phobos is currently migrating inward toward Mars on a relatively short timescale of  $\sim 70$  Myr, and it will likely tidally disrupt and form rings in the future (Black & Mittal 2015). It has been suggested that this process has occurred repeatedly throughout Mars's history, so that Mars has alternatively had a moon or rings on timescales of  $\sim 100$  Myr (Hesslebrock & Minton 2017). In other theoretical work, it has been suggested that the combined tides of a moon and parent star on an exoplanet can in some cases send the moon migrating into the planet until it is tidally disrupted and forms rings (Counselman 1973; Barnes & O'Brien 2002; Sasaki et al. 2012; Piro 2018). Thus, determining the presence or absence of rings may be an important probe of a planet's history.

In principle, rings should be detectable from detailed photometric or spectroscopic changes to transits that are strongest during ingress and egress (e.g., Barnes & Fortney 2004; Ohta et al. 2009; Zuluaga et al. 2015). The difficulty is that such signals are subtle and can be difficult to discern in current data. In a few cases, potential rings or at least constraints on rings have been made in this way (Heising et al. 2015; Aizawa et al. 2017), and in at

least one case it has been argued that an exoplanet has a giant ring system from a series of complex eclipses (Kenworthy & Mamajek 2015; Rieder & Kenworthy 2016), but this work has largely focused on giant planets rather than the rocky planets discussed here.

Ignoring these details, the simplest impact of rings would be to increase the depth of transits such that instead of measuring the planet radius  $R_p$ , an eclipsed area of  $A$  will result in an inferred radius of

$$R_{\text{inf}} = (A/\pi)^{1/2} \gtrsim R_p. \quad (1)$$

Thus if a population of exoplanets are found with seemingly anomalous radii, for example, because the exoplanets have densities that are too low (Zuluaga et al. 2015), this may indicate we are observing  $R_{\text{inf}}$  rather than  $R_p$ . Potentially connected with this is the issue of exoplanets with radii larger than Earth but smaller than Neptune (Batalha et al. 2013). There are no direct analogs of such planets in our solar system, which has led to interest in their origin. At least for the planets with radii  $\gtrsim 1.6 R_{\oplus}$ , the so-called sub-Neptunes, radial velocity measurements (Marcy et al. 2014) and detailed transit timing modeling (Wu & Lithwick 2013; Hadden & Lithwick 2014, 2017) reveal that most of these planets have low densities inconsistent with a purely rocky composition. The likely explanation is that they have extended, gaseous envelopes (Weiss & Marcy 2014; Rogers 2015), but given that rings could also increase the radius without increasing the mass appreciably, it seems like this is another option that should be considered.

Motivated by these issues, here I explore the inferred radii of rocky planets if there is a population with rings. In Section 2, I discuss the properties of these rings, focusing on their expected size and lifetime. In Section 3, I derive the eclipsed area of an exoplanet with rings as a function of the ring properties and viewing angle. In Section 4, I perform Monte Carlo calculations to under-

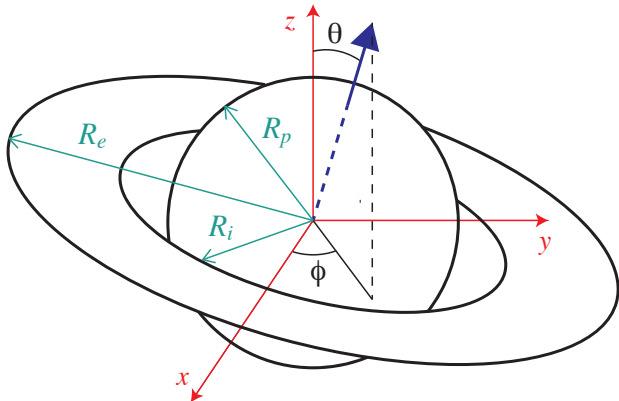


FIG. 1.— Planet with radius  $R_p$  encircled by rings with inner and out edge radii  $R_i$  and  $R_e$ , respectively. It is assumed that  $R_e \approx a_{\text{FRL}}$ , the fluid Roche limit, and that  $R_i \approx R_e/2$ , similar to Saturn’s rings. For an observer sitting along the  $x$ -axis, the tilt of the rings can be described by two angles, the obliquity with respect to the  $z$ -axis,  $\theta$ , and the azimuthal twist,  $\phi$ . The orientation of the rings is represented by the normal vector shown by the thick blue arrow. The area seen by the observer is simply this normal vector projected onto the  $x$ -axis, thus the effective area of just the rings is  $\pi(R_e^2 - R_i^2) \sin \theta |\cos \phi|$ .

stand the distribution of inferred radii for a population of ringed exoplanets, which are then compared to observations of super-Earths and sub-Neptunes in Section 5. Finally, I conclude in Section 6 with a summary of this work and a discussion of future areas to investigate.

## 2. SIZE AND LIFETIME OF A ROCKY RING

Following a scenario that may generate rings around a rocky planet (e.g., [Hesslebrock & Minton 2017](#); [Piro 2018](#)), the ring material will spread due to viscous effects. This can be the result of a combination of self-gravity wakes and local collisional processes ([Salmon et al. 2010](#)). Here I address whether rings should last for a sufficiently long time to be observationally important.

Rings as pictured in Figure 1 will viscously spread out until the outer edge  $R_e$  reaches the fluid Roche limit ([Murray & Dermott 1999](#))

$$R_e = a_{\text{FRL}} \approx 2.46 R_p \left( \frac{\rho_p}{\rho} \right)^{1/3}, \quad (2)$$

where  $\rho_p$  is the bulk density of the planet ( $\rho_p \approx 5.5 \text{ g cm}^{-3}$  for the Earth) and  $\rho$  is the density of particles that make up the rings. This density should not be confused with the rings themselves but rather the individual particles. Since the rings are envisioned as being rocky, a characteristic density of  $\rho \approx 2 \text{ g cm}^{-3}$  will be used, motivated by the type of material that makes up Phobos. Outside of the radius  $a_{\text{FRL}}$ , material will aggregate into satellites and no longer be part of the ring.

A key point is that the rings evolve in a self-similar way with time. This means that the evolution is rather quick at early times, and its final state is not too sensitive to the initial conditions (for example, see the ring evolution solutions of [Salmon et al. 2010](#)). Thus  $R_e$  quickly reaches  $a_{\text{FRL}}$ , and this can be approximated as the outer ring radius for the majority of its lifetime. Assuming that the densities of planets and ring material do not vary strongly, then  $R_e$  is simply proportional to the radius of the planet (and anyway, the density dependence is

weakened because of the cube root). In addition, there is the inner radius of the rings  $R_i$ , the exact value of which is less certain than  $R_e$ . Similar to the rings of Saturn, I will approximate  $R_i \approx R_e/2$ , although the exact value for  $R_i$  does not qualitatively change any of the conclusions in this work.

This self-similar evolution is also important for understanding the lifetime over which the rings are expected to be optically thick, since the total lifetime will be dominated by the viscous timescale at the latest stages. For rings with a surface density  $\Sigma$  composed of particles with radius  $r$  and density  $\rho$ , the optical depth is

$$\tau \approx \Sigma / r \rho. \quad (3)$$

Thus if the rings are marginally optically thick with  $\tau \approx 1$ , then  $\Sigma \approx r \rho$ , and the total mass of the rings from inner radius  $R_i$  to outer edge  $R_e$  is

$$\begin{aligned} M_r &\approx \pi \Sigma (R_e^2 - R_i^2) \approx 3\pi r \rho R_e^2 / 4 \\ &\approx 1.3 \times 10^{21} r_{100} \rho_2 \left( \frac{R_p}{R_\oplus} \right)^2 \left( \frac{\rho_p}{\rho} \right)^{2/3} \text{ g}, \end{aligned} \quad (4)$$

where  $r_{100} = r/100 \text{ cm}$ ,  $\rho_2 = \rho/2 \text{ g cm}^{-3}$ , and  $R_\oplus$  is the radius of Earth. As a comparison, this is about two orders of magnitude more mass than Phobos, about 5% of the mass of Saturn’s rings, or about 0.1% of the mass of Ceres.

The nature of the viscous evolution changes greatly depending on whether the ring is self-gravitating or not. This is measured by the Toomre  $Q$  parameter ([Toomre 1964](#))

$$Q = \frac{\Omega \sigma_r}{3.36 G \Sigma}, \quad (5)$$

where  $\Omega = (GM_p/R_e^3)^{1/2}$  is the orbital frequency and  $\sigma_r$  is the particle radial velocity dispersion. Roughly speaking, a ring will be gravitationally unstable for  $Q \lesssim 1$ , although even for  $Q \lesssim 2$  N-body simulations show that gravitational wakes can be effective at transporting angular momentum ([Salo 1995](#)). The velocity dispersion is regulated to roughly be the particle’s escape velocity,

$$\sigma_r \approx (4\pi G \rho / 3)^{1/2} r \approx 7.5 \times 10^{-2} r_{100} \rho_2^{1/2} \text{ cm s}^{-1}, \quad (6)$$

and the characteristic orbital frequency is

$$\Omega \approx 3.2 \times 10^{-4} \left( \frac{M_p}{M_\oplus} \right)^{1/2} \left( \frac{R_p}{R_\oplus} \right)^{-3/2} \left( \frac{\rho_p}{\rho} \right)^{-1/2} \text{ s}^{-1}, \quad (7)$$

where  $M_\oplus$  is the mass of the Earth. Putting these together,

$$Q \approx 0.54 \rho_2^{1/2} \left( \frac{M_p}{M_\oplus} \right)^{1/2} \left( \frac{R_p}{R_\oplus} \right)^{-3/2} \left( \frac{\rho_p}{\rho} \right)^{-1/2}. \quad (8)$$

Thus the ring is likely gravitational unstable in the outer parts and the self-gravity wakes will provide large scale transportation of angular momentum. Using the results of [Daisaka et al. \(2001\)](#), the associated self-gravity viscosity can be approximated as

$$\nu_{\text{SG}} = 13 \left( \frac{r_{\text{H}}}{2r} \right)^5 \left( \frac{G^2 \Sigma^2}{\Omega^3} \right), \quad (9)$$

where

$$r_H = \left( \frac{8\pi\rho r^3}{9M_p} \right)^{1/3} R_d, \quad (10)$$

is the particle's Hill radius. The ratio of this radius to the particles radius is

$$\frac{r_H}{r} = 1.54\rho_2^{1/3} \left( \frac{M_p}{M_\oplus} \right)^{-1/3} \left( \frac{R_p}{R_\oplus} \right) \left( \frac{\rho_p}{\rho} \right)^{1/3}. \quad (11)$$

The fact that  $r_H/r \gtrsim 1$  justifies the use of the particle's escape velocity for  $\sigma_r$  in Equation (6), otherwise, if  $r_H/r \lesssim 1$ , then the velocity dispersion would be dominated by the relative Keplerian velocity between particles  $\approx 2r\Omega$  (Daisaka et al. 2001). The viscosity is then

$$\begin{aligned} \nu_{\text{SG}} &= 18.7r_{100}^2\rho_2^{11/3} \left( \frac{M_p}{M_\oplus} \right)^{-19/6} \\ &\times \left( \frac{R_p}{R_\oplus} \right)^{19/2} \left( \frac{\rho_p}{\rho} \right)^{19/6} \text{ cm}^2 \text{ s}^{-1}. \end{aligned} \quad (12)$$

Another possibility is that angular momentum can be transported via sound waves traveling between colliding particles, which has an associated viscosity (Araki & Tremaine 1986; Wisdom & Tremaine 1988)

$$\begin{aligned} \nu_{\text{col}} &= r^2\Omega\tau \\ &= 3.2r_{100}^2 \left( \frac{M_p}{M_\oplus} \right)^{1/2} \left( \frac{R_p}{R_\oplus} \right)^{-3/2} \left( \frac{\rho_p}{\rho} \right)^{-1/2} \text{ cm}^2 \text{ s}^{-1}, \end{aligned} \quad (13)$$

where again  $\tau \approx 1$  is assumed. Since  $\nu_{\text{col}} \lesssim \nu_{\text{SG}}$ , the viscous timescale is dominated by the self-gravity effects. Thus, the timescale for the ring to viscously evolve is estimated as

$$\begin{aligned} t_{\text{visc}} &\approx R_d^2/\nu_{\text{SG}} \\ &\approx 4.2 \times 10^9 r_{100}^{-1} \rho_2^{-11/3} \left( \frac{M_p}{M_\oplus} \right)^{19/6} \\ &\times \left( \frac{R_p}{R_\oplus} \right)^{-15/2} \left( \frac{\rho_p}{\rho} \right)^{-5/2} \text{ yr}. \end{aligned} \quad (14)$$

Since for rocky planets it is expected that  $\rho_p/\rho \gtrsim 1$ , a typical viscous timescale is a few 100 Myr. This demonstrates that once formed, these rings are expected to be optically thick for a significant amount of time. This is similar to the timescales found in more detailed simulations for hypothesized rings around Mars during its previous history (Hessbrock & Minton 2017).

### 3. ECLIPSED AREA OF A RINGED EXOPLANET

Next, I consider the area an exoplanet with rings eclipses from the point of view of an observer watching a transit. As shown in Figure 1, the parent star, exoplanet, and observer are assumed to approximately sit in the same  $xy$ -plane since eclipses only occur for a small range of separation angles  $\approx R_*/D \ll 1$ , where  $R_*$  is the star's radius and  $D$  is the distance between the star and exoplanet. The orientation of the ring with respect to the observer depends on two angles. These are the obliquity  $\theta$ , which is measured from the  $z$ -axis perpendicular

to the exoplanet's orbit, and the azimuthal angle  $\phi$  (also sometimes referred to as the "season"). With these definitions, the values of these angles run from  $0 \leq \theta \leq \theta_{\text{obl}}$ , where  $\theta_{\text{obl}}$  is the maximum possible obliquity for these systems, and  $0 \leq \phi \leq 2\pi$ .

To an observer, the inner and outer edge of the ring appear as an ellipses with semi-major axes  $a_i = R_i$  and  $a = R_e$ , respectively, and semi-minor axes  $b_i = R_i \sin \theta |\cos \phi|$  and  $b_e = R_e \sin \theta |\cos \phi|$ , respectively. The total area blocked by the ring is thus  $\pi(a_e b_e - a_i b_i) = \pi(R_e^2 - R_i^2) \sin \theta |\cos \phi|$ , while the exoplanet will block out an area  $\pi R_p^2$ . This does not take into account that there are regions where the ring and planet overlap from the observer's point of view. To address this, three different cases are considered (see Figure 2).

#### 3.1. Case A: $b_i > R_p$

As shown in the top diagram of Figure 2, this is the simplest case where there is no overlap between the planet and the ring. Here the blocked area is

$$A = \pi(R_e^2 - R_i^2) \sin \theta |\cos \phi| + \pi R_p^2, \quad (15)$$

which is simply the sum of the two areas.

#### 3.2. Case B: $b_e > R_p > b_i$

As shown in the middle diagram of Figure 2, in this case the planet will cross over the inner edge of the ring, but does not extend beyond the ring's outer edge. First, there is the area covered by the ring, which just like before has a projected area of  $\pi(R_e^2 - R_i^2) \sin \theta |\cos \phi|$ . Then, there is the remaining area covered by the planet. This can be divided into four sectors, two of which are highlighted in light blue and green. The area of the light blue sector can be found using Cavallieri's principle to be

$$\text{Blue sector} = \frac{\alpha_i}{2} a_i b_i = \frac{\alpha_i}{2} R_i^2 \sin \theta |\cos \phi|, \quad (16)$$

while the green sector is just a fraction of a circle

$$\text{Green sector} = \frac{\pi - \alpha_i}{2} R_p^2. \quad (17)$$

The angle  $\alpha_i$  can be found using some trigonometry. First note that the distance  $d_i$  is given by

$$d_i = 2a_i \left( \frac{R_p^2 - b_i^2}{a_i^2 - b_i^2} \right)^{1/2}. \quad (18)$$

Thus the angle is

$$\alpha_i = 2 \arcsin \left[ \frac{a_i}{R_p} \left( \frac{R_p^2 - b_i^2}{a_i^2 - b_i^2} \right)^{1/2} \right]. \quad (19)$$

Putting this all together,

$$\begin{aligned} A &= \pi(a_e b_e - a_i b_i) + \alpha_i a_i b_i + (\pi - \alpha_i) R_p^2, \\ &= \pi(R_e^2 - R_i^2) \sin \theta |\cos \phi| + \alpha_i R_i \sin \theta |\cos \phi| \\ &\quad + (\pi - \alpha_i) R_p^2. \end{aligned} \quad (20)$$

is the total observed area.

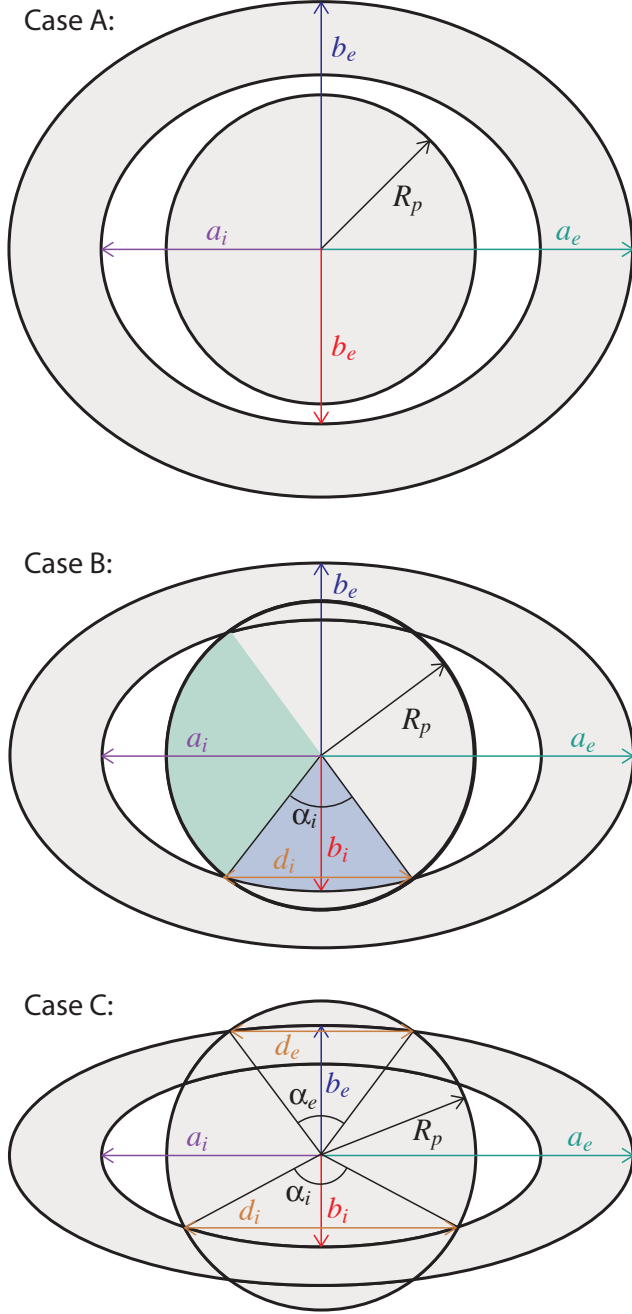


FIG. 2.— Diagrams of the area covered by a planet plus ring. The ring has inner and outer edge radii  $R_i$  and  $R_e$ , respectively. When viewed with obliquity  $\theta$  from an angle  $\phi$ , these form ellipses with semi-major axes  $a_i = R_i$  and  $a = R_e$ , respectively, and semi-minor axes  $b_i = R_i \sin \theta |\cos \phi|$  and  $b_e = R_e \sin \theta |\cos \phi|$ , respectively. To simplify assessing the area, three separate cases are considered, Case A when  $b_i > R_p$ , Case B when  $b_e > R_p > b_i$ , and Case C when  $R_p > b_e$ . Other key angles and distances labeled in the panels are further described in the text.

### 3.3. Case C: $R_p > b_e$

In the final case, the planet extends further than the outer edge of the ring from the observer's view. If the inner radius of the ring is ignored, one can find the area of the outer outline in the bottom panel of Figure 2. This is composed of two elliptical sectors (on the left and right) and two circular sectors (on the top and bottom). Again

using Cavalieri's principle,

$$\text{Area of outer shape} = (\pi - \alpha_e)a_e b_e + \alpha_e R_p^2, \quad (21)$$

where in analogy with the derivation of  $a_i$  above, one can first find the length

$$d_e = 2a_e \left( \frac{R_p^2 - b_e^2}{a_e^2 - b_e^2} \right)^{1/2}, \quad (22)$$

to find the angle

$$\alpha_e = 2 \arcsin \left[ \frac{a_e}{R_p} \left( \frac{R_p^2 - b_e^2}{a_e^2 - b_e^2} \right)^{1/2} \right]. \quad (23)$$

The area of the inner ring then needs to be subtracted. This is done by subtracting the total elliptical sectors on the left and right and then adding back the area covered by the planet

$$\text{Area of inner holes} = (\pi - \alpha_i)a_i b_i - (\pi - \alpha_i)R_p^2, \quad (24)$$

where  $\alpha_i$  is the same as given by Equation (19) above. Putting this all together,

$$\begin{aligned} A &= (\pi - \alpha_e)a_e b_e - (\pi - \alpha_i)a_i b_i + (\pi + \alpha_e - \alpha_i)R_p^2, \\ &= (\pi - \alpha_e)R_e^2 \sin \theta |\cos \phi| - (\pi - \alpha_i)R_i^2 \sin \theta |\cos \phi| \\ &\quad + (\pi + \alpha_e - \alpha_i)R_p^2, \end{aligned} \quad (25)$$

is the total projected area.

### 3.4. Inferred Radius

If a transit is observed and the eclipse depth provides an area  $A$  for the planet, then the inferred radius of the planet is given by Equation (1). As shown for the values of  $A$  derived above for a planet with rings, it is always the case that  $R_{\text{inf}} > R_p$ . This is further shown in Figure 3, where  $R_{\text{inf}}$  is plotted for different values of  $\theta$  and  $\phi$  (also see Figure 1 from Heising et al. 2015, which shows example schematics for how the rings appear from different angles). At small  $\theta$ , the ring is viewed nearly edge on and thus  $R_{\text{inf}}/R_p \approx 1$ . As  $\theta$  increases, so does  $R_{\text{inf}}$  until reaching a maximum value when face on. Although  $R_{\text{inf}}$  changes continuously, kinks are seen as  $R_{\text{inf}}$  transitions through the three cases, starting at Case C (when  $\theta$  is small) and ending with Case A (when  $\theta$  is large, although note that not all three cases are covered when  $\phi$  is sufficiently large).

These results assume that the rings are optically thick to the star light, but this assumption is justified for two reasons. First, the timescale discussion in Section 2 shows that it is plausible for the rings to remain optically thick for  $\gtrsim 10^9$  yrs. Second, the rings will in general be viewed from an angle different than exactly face on. The optical depth through the rings viewed at an angle is greater because the thickness along the observer's path is larger, so that it is more likely that the rings will appear optically thick.

## 4. MONTE CARLO CALCULATIONS

Although the impact of rings on a single transit may be subtle, a large collection of transits will show a component of anomalously large radii from a population of

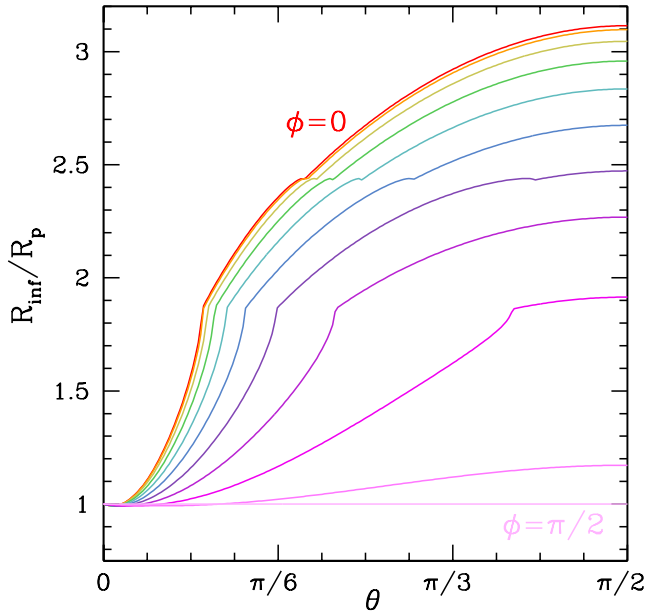


FIG. 3.— Inferred radius  $R_{\text{inf}}$  for a planet with rings viewed at different angles  $\theta$ . Colors curves go from  $\phi = 0$  (red) to  $\phi = \pi/2$  (light pink) in increments of  $\pi/20$ . The rings are chosen to have inner and outer edge radii of  $R_i = 1.72R_p$  and  $R_e = 3.44R_p$ , respectively.

rings. Since there is a large range of parameters and distributions for the planetary properties, here I explore different possibilities using Monte Carlo calculations and summarize the impact on the distributions of  $R_{\text{inf}}$ .

The general strategy is to start with a probability density for the planetary radii

$$P(R_p) \propto R_p^{-\eta}, \quad (26)$$

which is defined such that

$$\int_{R_1}^{R_2} P(R_p) dR_p = 1, \quad (27)$$

where  $R_1$  and  $R_2$  are the minimum and maximum radii of rocky exoplanets. These are very uncertain, and although  $R_1 = 0.7R_{\oplus}$  and  $R_2 = 1.3R_{\oplus}$  is chosen for this work, this should be updated as this distribution is better understood. See the Appendix for further details on how  $P(R_p)$  is implemented.

Using Equation (2), the corresponding outer ring radius  $R_e$  is estimated from a given  $R_p$ . The inner edge is less clear and for this work it is estimated as  $R_i \approx R_e/2$ , which is similar to Saturn's rings. For the angles, flat distributions in  $0 \leq \phi \leq 2\pi$  and  $0 \leq \theta \leq \theta_{\text{obl}}$  are considered. The transiting area is calculated using the three cases outlined in Section 3, and then I find  $R_{\text{inf}}$  using Equation (1). Typically  $5 \times 10^6$  exoplanets are run to make sure the distributions converge. The histograms presented are made with logarithmically spaced bins, motivated by the work of [Fulton et al. \(2017\)](#) on the radius distribution of small planets from California-*Kepler* Survey (further discussed in Section 5). Such binning puts additional emphasis on the larger radii to highlight additional features that might be less apparent with more evenly distributed binning.

A first example of a histogram of inferred radii is shown

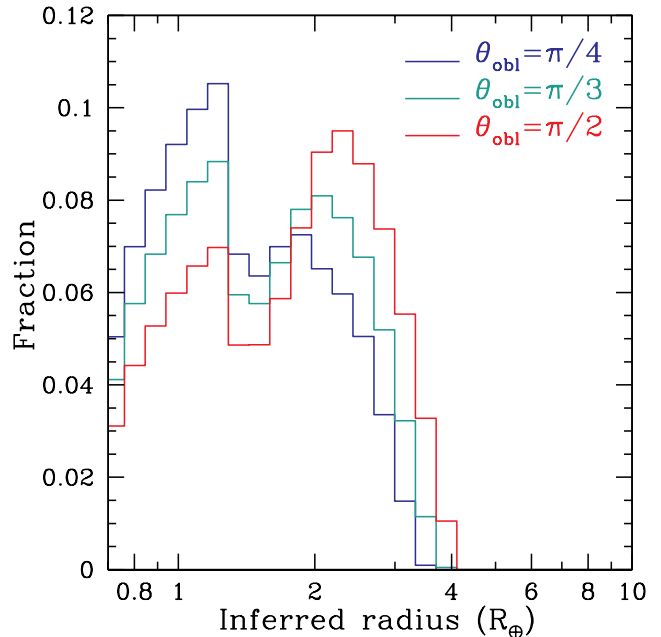


FIG. 4.— Example inferred radius distributions for a population of rocky planets with rings for different maximum obliquities  $\theta_{\text{obl}}$ . This assumes a log-normal distribution for the planetary radii  $P(R_p) \propto R_p^{-1}$  with a range of  $0.7 \leq R_p/R_{\oplus} \leq 1.3$ , along with flat distributions in  $0 \leq \phi \leq 2\pi$  and  $0 \leq \theta \leq \theta_{\text{obl}}$ . The inner and outer edge of the rings have radii  $R_i = 1.72R_p$  and  $R_e = 3.44R_p$ , respectively, which is appropriate for bulk densities for the planet and rings of  $\rho_p = 5.5 \text{ g cm}^{-3}$  and  $\rho = 2 \text{ g cm}^{-3}$ , respectively. All planets are assumed to have rings.

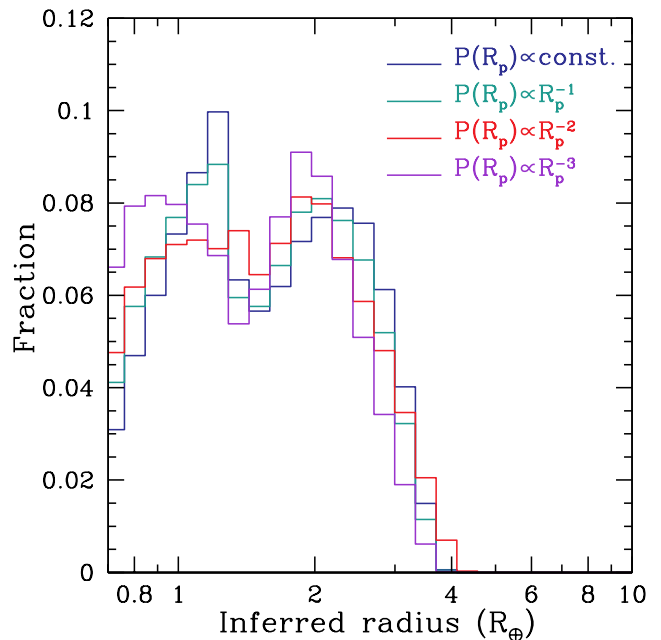


FIG. 5.— Similar to Figure 4, but with a fixed value of  $\theta_{\text{obl}} = \pi/3$  and different distributions for the exoplanet radii (see text and Appendix for a full description of these distributions).

in Figure 4. Here it is assumed that all exoplanets have rings and that  $P(R_p) \propto R_p^{-1}$ . The maximum obliquity  $\theta_{\text{obl}}$  is varied to better understand how this impacts the distribution of inferred radii. The obliquity of the planets in our solar system vary greatly, so three characteristic



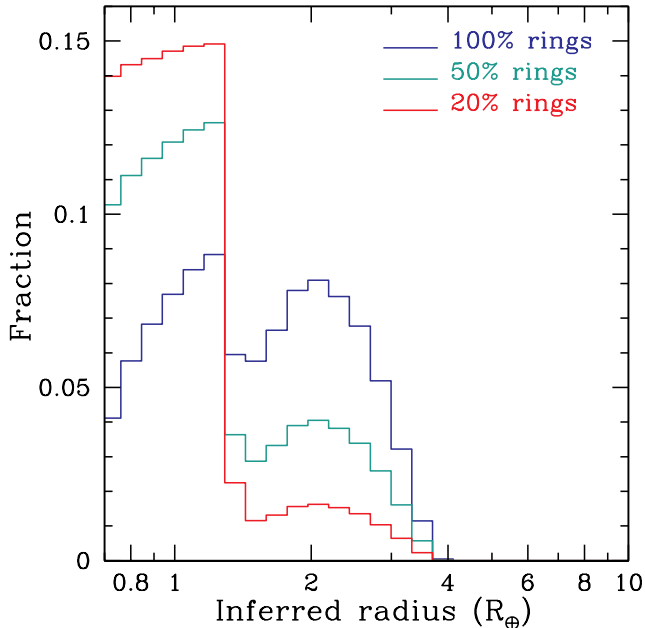


FIG. 6.— Similar to Figure 4, but with a fixed value of  $\theta_{\text{obl}} = \pi/3$  and  $P(R_p) \propto R_p^{-1}$  with different fraction of planets with rings as labeled.

values are considered as denoted in Figure 4. These examples show that a bimodal distribution of radii is generally expected when rings are present. This is because there is one larger radius peak from the average viewing angle of the rings, but in addition, there is a smaller radius peak from the nearly edge-on exoplanets where the transit is dominated by the exoplanet radius itself. The large radius peak increases in size and average value of  $R_{\text{inf}}$  with increasing  $\theta_{\text{obl}}$  because this results in more systems with rings closer to face on.

In Figure 5, I explore how the assumed planet distribution changes the bimodal distribution due the presence of rings. The main change is that a flatter distribution of  $R_p$  results in a slightly larger value for the peak  $R_{\text{inf}}$ , although this effect is more subtle than changing  $\theta_{\text{obl}}$  (see Figure 4). At the low radius end, the radius distribution can be studied more directly, so that in the future hopefully this distribution can be constrained for input into studies such as the one here.

In the previous example, all planets are assumed to have rings, but this is clearly too optimistic. In Figure 5, I explore how the distributions change when only some fraction of planets have rings. Here,  $\theta_{\text{obl}} = \pi/3$  and  $P(R_p) \propto R_p^{-1}$  and three different fractions of planets with rings are considered. Not surprisingly, the lower radius peak increases dramatically when the number of planets without rings is increased. This means that it is unlikely that the two peak in the radius distribution are comparable, unless there is a significant number of planets with rings.

## 5. COMPARISON TO SMALL PLANET OBSERVATIONS

As mentioned in Section 1, one of the developing areas in exoplanet studies is the large number of planets smaller than Neptune discovered by the *Kepler* mission. These were not predicted by initial theories of planet formation (e.g., [Ida & Lin 2004](#); [Mordasini et al. 2009](#)),

which expected that planets should either fail to accrete enough material to become super-Earths or grow quickly and efficiently to form gas-rich giants. More recent formation models are now able to produce super-Earths as observed (e.g., [Hansen & Murray 2012](#); [Mordasini et al. 2012](#); [Alibert et al. 2013](#); [Chiang & Laughlin 2013](#); [Chatterjee & Tan 2014](#); [Coleman & Nelson 2014](#); [Lee et al. 2014](#); [Raymond & Cossou 2014](#); [Lee & Chiang 2016](#)), and in particular, now highlight the important role atmospheric erosion by photoevaporation can play in the planet radii distribution (e.g., [Owen & Wu 2013](#); [Jin et al. 2014](#); [Lopez & Fortney 2014](#); [Chen & Rogers 2016](#); [Lopez & Rice 2016](#); [Owen & Wu 2017](#)). Such models predict a dearth of intermediate sub-Neptune planets in highly irradiated environments. This is because a small envelope of H/He can greatly inflate a planet’s radius, so that the result is either a bare rocky cores with a small radius or a rocky core with a small envelope but much larger radius ([Lopez & Fortney 2014](#)). It was therefore interesting to see, using the subsample of planets from the California-*Kepler* Survey ([Johnson et al. 2017](#); [Petigura et al. 2017, 2018](#); [Weiss et al. 2018](#)), a deficit in the occurrence rate distribution at a radius of  $\approx 1.5 - 2.0 R_{\oplus}$  ([Fulton et al. 2017](#)), somewhat consistent with this picture (although see [Bouma et al. 2018](#) and [Teske et al. 2018](#) for discussions on uncertainties in this distribution, depending on the presence of unseen companion stars).

Nevertheless, the exact explanation for the presence of such a H/He envelope and the resulting distribution of radii is still uncertain. It could indeed be due to photoevaporation losses, but there is currently not enough data on exoplanet radii as a function of insolation flux to test this idea in detail. Other mechanisms for getting a small H/He envelope on a rocky core include the delay of gas accretion due to dynamical friction in the protoplanetary disk ([Lee et al. 2014](#); [Lee & Chiang 2016](#)), a secondary atmosphere outgassed during planet formation and evolution ([Adams et al. 2008](#); [Elkins-Tanton & Seager 2008](#)), or erosion by impacts that significantly strip large primordial envelopes down to just a few percent of their initial mass ([Liu et al. 2015](#); [Schlichting et al. 2015](#); [Inamdar & Schlichting 2016](#)).

Although previous theoretical work provides many reasons to think the bimodal radius distribution could be related to the envelope masses, here I consider the speculative idea of whether it could be related to the presence of rings instead. Figure 4 demonstrates that a bimodal distribution in radii is expected from the presence of rings, but there are two difficulties. First, to get a sufficiently large secondary peak, the obliquity must be rather large with  $\theta_{\text{obl}} \approx \pi/2$ . This can be somewhat offset with a larger  $R_e$  and/or smaller  $R_i$  than I have chosen here. Given the uncertainties in these parameters, it is plausible that they are somewhat different than the fiducial values I assume. A second, potentially larger problem is that Figure 4 assumes that all rocky exoplanets have rings, which is almost certainly not the case. Furthermore, as Figure 6 demonstrates, when rings are only present for a subset of rocky planets, the first peak quickly grows large in comparison to the second. If this is the case, can this model at all be reconciled with the results of [Fulton et al. \(2017\)](#)?

To investigate this further, I plot the case when 50% of rocky exoplanets have rings with  $P(R_p) \propto R_p^{-1}$  and

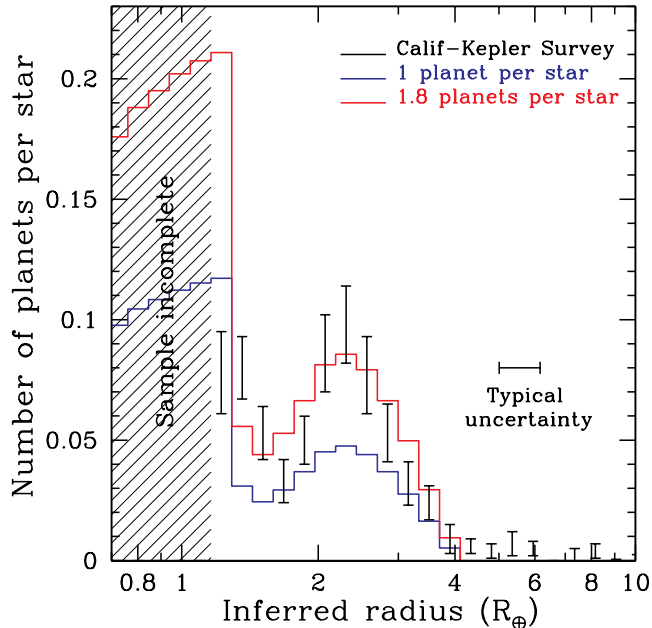


FIG. 7.— Comparison between the radius distribution of small planets from the California-*Kepler* Survey to a distribution of planets with rings where 50% of the planets have rings, with  $\theta_{\text{obl}} = \pi/2$  and  $P(R_p) \propto R_p^{-1}$ . Cases with 1 planet per star (blue histogram) and 1.8 planets per star (red histogram) are considered. Below a radius of  $1.16 R_{\oplus}$ , the sample is incomplete and not plotted.

$\theta_{\text{obl}} = \pi/2$  in Figure 7. Note that thus far I have been plotting the *fraction of all planets that have a certain radius*, whereas [Fulton et al. \(2017\)](#) considers the *fraction of all stars that have a planet with a certain radius*. To make the conversion requires understanding the average number of small planets per star ([Howard et al. 2010](#); [Mayor et al. 2011](#); [Howard et al. 2012](#); [Dong & Zhu 2013](#); [Fressin et al. 2013](#); [Petigura et al. 2013](#); [Burke et al. 2015](#); [Dressing & Charbonneau 2015](#)), and since this is uncertain, in Figure 7 I consider two characteristic values of 1 planet per star (blue histogram, which does not fit the second peak) and 1.8 planets per star (red histogram, which better represents the data).

This shows that although there are many uncertainties and free parameters that can be varied, in principle, rings can explain the secondary peak in these exoplanet radii. There are main two potential issues with this. First, it requires that on the order of  $\sim 50\%$  of rocky exoplanets need rings. Although this is not 100%, it still may be uncomfortably large. On the other hand, once a rocky exoplanet has rings, they could last for a consider amount of time (see the discussion in Section 2). Second, to get the correct fraction of exoplanets with inferred radii in the range  $\approx 2 - 3 R_{\oplus}$  implies a much larger fraction of planets per star in the range below  $\lesssim 1.2 R_{\oplus}$ . Currently, radius measurements are incomplete at small radii, but perhaps not at a large enough level to provide the large amount of  $\lesssim 1.2 R_{\oplus}$  exoplanets needed here.

Alternatively, this work may simply suggest that the sub-Neptunes are subject to contamination by ringed rocky exoplanets, but this may not explain the majority of these objects. These sub-Neptunes therefore should be subject to greater scrutiny to establish their true nature.

## 6. CONCLUSIONS AND DISCUSSION

Although rocky planets with rings do not exist in our Solar System, it has not been established whether this is true or not for exoplanets. Motivated by theoretical studies that suggest that at least some rocky exoplanets should have rings (e.g., [Hesslebrock & Minton 2017](#); [Barnes & O’Brien 2002](#); [Piro 2018](#)), here I explored what the inferred distribution of radii would be for rocky exoplanets if such rings existed. The main conclusion is that rings lead to an inferred (rather than actual) radius distribution with two peaks, with the first peak being from the intrinsic radius distribution of rocky exoplanets and the second peak from the rings transiting at an average viewing angle. The exact details of this distribution depend on many uncertain factors, such as the underlying radius distribution of rocky exoplanets, the radii of the inner and outer edges of the rings, and the distribution of obliquities of small exoplanets. These are all varied and explored in this work to provide better intuition on how they impact the resulting inferred radius distribution.

Furthermore, I discuss the expected lifetime of these rings assuming that they can form, which is found to be  $\gtrsim 10^9$  yrs. This makes it at least plausible that the rings can be present for a non-negligible fraction of rocky exoplanets. In detail, these rings may come and go and alternatively be moons instead as the ring undergoes viscous evolution and gravitational instabilities, so more sophisticated time dependent models should be developed to address the duty cycle for these rings in detail.

I also consider the speculative idea of whether the secondary peak in the radii of small planets ([Fulton et al. 2017](#)) can be explained by the presence of rings. This is potentially difficult, but not ruled out. As shown by Figure 7, a rather extreme obliquity of  $\theta_{\text{obl}} \approx \pi/2$  is needed. In addition, to get a sufficient fraction of inferred radii in the range  $\approx 2 - 3 R_{\oplus}$  requires an even larger fraction of small radii  $\lesssim 1.2 R_{\oplus}$ , which may be difficult to reconcile with exoplanet measurements.

Even if this model cannot completely explain the secondary peak in the range of  $\approx 2 - 3 R_{\oplus}$ , it suggests that rings could be an important contaminate. Therefore, this radius range should be subject to further studies to address the fraction of rocky exoplanets with rings. Probably the best way to distinguish between rings and the favored scenario of an inflated H/He envelope would be via transmission spectroscopy. It may be difficult to definitively determine if there are rings in this way, since both rocky rings and a cloudy atmosphere would be rather wavelength independent. Nevertheless, evidence for rings around rocky exoplanets would be another amazing way that extrasolar planetary systems differ from our own.

I thank Johanna Teske for pointing out the small planet radius gap issue and providing feedback on a previous draft. I also thank Tiffany Meshkat for helpful discussions, and Jason Barnes for bringing to my attention the inward migration of Phobos, which helped inspire this work.

APPENDIX  
PROBABILITY DISTRIBUTIONS

For the Monte Carlo runs, I use a probability density for the planetary radius distribution,

$$P(R_p) \propto R_p^{-\eta}. \quad (\text{A1})$$

which is defined such that

$$\int_{R_1}^{R_2} P(R_p) dR_p = 1, \quad (\text{A2})$$

where  $R_1$  and  $R_2$  are the smallest and large radii for the distribution of planets, respectively. Here for completeness I describe how this is implemented.

A random number  $\Psi$  is chosen to be between 0 and 1. From this the planet radius for  $\eta = 0$  is given as

$$R_p = R_1 + (R_2 - R_1)\Psi, \quad (\text{A3})$$

for  $\eta = 1$

$$R_p = R_1 \exp \left[ \ln \left( \frac{R_2}{R_1} \right) \Psi \right], \quad (\text{A4})$$

and for  $\eta > 1$

$$R_p = \left[ \frac{1}{R_1^{\eta-1}} - \left( \frac{1}{R_1^{\eta-1}} - \frac{1}{R_2^{\eta-1}} \right) \Psi \right]^{-1/(\eta-1)}. \quad (\text{A5})$$

The random number  $\Psi$  is generated using the RAN2 routine from [Press et al. \(1992\)](#).

REFERENCES

- Adams, E. R., Seager, S., & Elkins-Tanton, L. 2008, *ApJ*, 673, 1160
- Aizawa, M., Uehara, S., Masuda, K., Kawahara, H., & Suto, Y. 2017, *AJ*, 153, 193
- Alibert, Y., Carron, F., Fortier, A., et al. 2013, *A&A*, 558, A109
- Araki, S., & Tremaine, S. 1986, *Icarus*, 65, 83
- Barnes, J. W., & Fortney, J. J. 2004, *ApJ*, 616, 1193
- Barnes, J. W., & O'Brien, D. P. 2002, *ApJ*, 575, 1087
- Batalha, N. M., Rowe, J. F., Bryson, S. T., et al. 2013, *ApJS*, 204, 24
- Black, B. A., & Mittal, T. 2015, *Nature Geoscience*, 8, 913
- Bouma, L. G., Masuda, K., & Winn, J. N. 2018, *ArXiv e-prints*
- Burke, C. J., Christiansen, J. L., Mullally, F., et al. 2015, *ApJ*, 809, 8
- Chatterjee, S., & Tan, J. C. 2014, *ApJ*, 780, 53
- Chen, H., & Rogers, L. A. 2016, *ApJ*, 831, 180
- Chiang, E., & Laughlin, G. 2013, *MNRAS*, 431, 3444
- Coleman, G. A. L., & Nelson, R. P. 2014, *MNRAS*, 445, 479
- Counselman, III, C. C. 1973, *ApJ*, 180, 307
- Daisaka, H., Tanaka, H., & Ida, S. 2001, *Icarus*, 154, 296
- Dong, S., & Zhu, Z. 2013, *ApJ*, 778, 53
- Dressing, C. D., & Charbonneau, D. 2015, *ApJ*, 807, 45
- Elkins-Tanton, L. T., & Seager, S. 2008, *ApJ*, 685, 1237
- Fressin, F., Torres, G., Charbonneau, D., et al. 2013, *ApJ*, 766, 81
- Fulton, B. J., Petigura, E. A., Howard, A. W., et al. 2017, *AJ*, 154, 109
- Hadden, S., & Lithwick, Y. 2014, *ApJ*, 787, 80
- , 2017, *AJ*, 154, 5
- Hansen, B. M. S., & Murray, N. 2012, *ApJ*, 751, 158
- Heising, M. Z., Marcy, G. W., & Schlichting, H. E. 2015, *ApJ*, 814, 81
- Hesslebrock, A. J., & Minton, D. A. 2017, *Nature Geoscience*, 10, 266
- Howard, A. W., Marcy, G. W., Johnson, J. A., et al. 2010, *Science*, 330, 653
- Howard, A. W., Marcy, G. W., Bryson, S. T., et al. 2012, *ApJS*, 201, 15
- Ida, S., & Lin, D. N. C. 2004, *ApJ*, 604, 388
- Inamdar, N. K., & Schlichting, H. E. 2016, *ApJ*, 817, L13
- Jin, S., Mordasini, C., Parmentier, V., et al. 2014, *ApJ*, 795, 65
- Johnson, J. A., Petigura, E. A., Fulton, B. J., et al. 2017, *AJ*, 154, 108
- Kenworthy, M. A., & Mamajek, E. E. 2015, *ApJ*, 800, 126
- Lee, E. J., & Chiang, E. 2016, *ApJ*, 817, 90
- Lee, E. J., Chiang, E., & Ormel, C. W. 2014, *ApJ*, 797, 95
- Liu, S.-F., Hori, Y., Lin, D. N. C., & Asphaug, E. 2015, *ApJ*, 812, 164
- Lopez, E. D., & Fortney, J. J. 2014, *ApJ*, 792, 1
- Lopez, E. D., & Rice, K. 2016, *ArXiv e-prints*
- Marcy, G. W., Isaacson, H., Howard, A. W., et al. 2014, *ApJS*, 210, 20
- Mayor, M., Marmier, M., Lovis, C., et al. 2011, *ArXiv e-prints*
- Mordasini, C., Alibert, Y., & Benz, W. 2009, *A&A*, 501, 1139
- Mordasini, C., Alibert, Y., Georgy, C., et al. 2012, *A&A*, 547, A112
- Mulders, G. D., Pascucci, I., & Apai, D. 2015, *ApJ*, 798, 112
- Murray, C. D., & Dermott, S. F. 1999, *Solar system dynamics*
- Ohta, Y., Taruya, A., & Suto, Y. 2009, *ApJ*, 690, 1
- Owen, J. E., & Wu, Y. 2013, *ApJ*, 775, 105
- , 2017, *ApJ*, 847, 29
- Petigura, E. A., Howard, A. W., & Marcy, G. W. 2013, *Proceedings of the National Academy of Science*, 110, 19273
- Petigura, E. A., Howard, A. W., Marcy, G. W., et al. 2017, *AJ*, 154, 107
- Petigura, E. A., Marcy, G. W., Winn, J. N., et al. 2018, *AJ*, 155, 89
- Piro, A. L. 2018, *ArXiv e-prints*
- Press, W. H., Teukolsky, S. A., Vetterling, W. T., & Flannery, B. P. 1992, *Numerical recipes in C. The art of scientific computing*
- Raymond, S. N., & Cossou, C. 2014, *MNRAS*, 440, L11
- Rieder, S., & Kenworthy, M. A. 2016, *A&A*, 596, A9
- Rogers, L. A. 2015, *ApJ*, 801, 41
- Salmon, J., Charnoz, S., Crida, A., & Brahic, A. 2010, *Icarus*, 209, 771
- Salo, H. 1995, *Icarus*, 117, 287
- Sasaki, T., Barnes, J. W., & O'Brien, D. P. 2012, *ApJ*, 754, 51
- Schlichting, H. E., Sari, R., & Yalinewich, A. 2015, *Icarus*, 247, 81
- Teske, J. K., Ciardi, D. R., Howell, S. B., Hirsch, L. A., & Johnson, R. A. 2018, *ArXiv e-prints*
- Toomre, A. 1964, *ApJ*, 139, 1217
- Weiss, L. M., & Marcy, G. W. 2014, *ApJ*, 783, L6
- Weiss, L. M., Marcy, G. W., Petigura, E. A., et al. 2018, *AJ*, 155, 48



- Wisdom, J., & Tremaine, S. 1988, AJ, 95, 925  
Wu, Y., & Lithwick, Y. 2013, ApJ, 772, 74  
Zuluaga, J. I., Kipping, D. M., Sucerquia, M., & Alvarado, J. A.  
2015, ApJ, 803, L14